Science Bulletin 64 (2019) 1757–1763

Contents lists available at ScienceDirect

Science Bulletin

journal homepage: www.elsevier.com/locate/scib

Science Bulletin
www.scibull.com

Article

Experimental demonstration of suppressing residual geometric dephasing

Jin-Ming Cui [a,b], Ming-Zhong Ai [a,b], Ran He [a,b], Zhong-Hua Qian [a,b], Xiao-Ke Qin [c], Yun-Feng Huang [a,b,*], Zheng-Wei Zhou [a,b,*], Chuan-Feng Li [a,b,*], Tao Tu [a,b], Guang-Can Guo [a,b]

[a] CAS Key Laboratory of Quantum Information, University of Science and Technology of China, Hefei 230026, China
[b] CAS Center For Excellence in Quantum Information and Quantum Physics, University of Science and Technology of China, Hefei 230026, China
[c] Luoyang Institute of Electro-Optical Equipment, AVIC, Luoyang 471000, China

ARTICLE INFO

Article history:
Received 3 July 2019
Received in revised form 1 August 2019
Accepted 23 August 2019
Available online 10 September 2019

Keywords:
Geometric dephasing
Berry phase
Dynamic decoupling
Ion trap

ABSTRACT

The geometric phase is regarded as a promising strategy in fault tolerance quantum information processing (QIP) domain due to its phase only depending on the geometry of the path executed. However, decoherence caused by environmental noise will destroy the geometric phase. Traditional dynamic decoupling sequences can eliminate dynamic dephasing but can not reduce residual geometric dephasing, which is still vital for high-precision quantum manipulation. In this work, we experimentally demonstrate effective suppression of residual geometric dephasing with modified dynamic decoupling schemes, using a single trapped $^{171}Yb^{+}$ ion. The experimental results show that the modified schemes can reduce dephasing rate up to more than one order of magnitude compared with traditional dynamic decoupling schemes, where residual geometric dephasing dominates. Besides, we also investigate the impact of intensity and correlation time of the low-frequency noise on coherence of the quantum system. And we confirm these methods can be used in many cases.

1. Introduction

The geometric phase, also known as Berry phase [1], associated with adiabatic and cyclic evolution of Hamiltonian in parameter space, plays a fundamental role in a broad range of physics applications, including precision measurement [2,3], Aharonnv-Anandan phase [4], mixed state [5] and non-unitary evolution [6]. Especially in quantum information processing (QIP) domain, Berry phase is deemed as a promising way to realize precise quantum control due to its nature of being immune to specific environmental noise. A number of platforms, such as nuclear magnetic resonance (NMR) [7], superconducting circuit [8,9], graphene [10], nitrogen-vacancy (NV) [11] and ultracold atoms [12,13], have done many meaningful research about Berry phase in past few decades. Among these research, high fidelity geometric phase gate based ion trap has made surprising progress in recent years: an entangled Bell state with 97% fidelity was prepared in Ref. [14]; the single geometric phase gates with fidelity above threshold required for fault-tolerant quantum computation have been achieved in Refs. [15,16], in which dephasing is the dominate gate error source. Because much fewer physical qubits are required to encode a logic qubit with higher gate fidelity, further suppressing the dephasing and improving control precision in single geometric phase gates become one of the most important task to realize practical fault-tolerant quantum computation.

Dephasing arising from the information correlation between the qubit system and its environment, causes randomization of the phase of the qubit, then the information stored in the qubit is ultimately lost [2,17]. One part of this dephasing is dynamic dephasing while the other part is from geometric origin [18]. Geometric dephasing is present even in the adiabatic limit and when no geometric phase is acquired [19]. Although dynamic dephasing can be suppressed through spin echo method [7], the residual geometric dephasing is difficult to eliminate. So, for the purpose of high fidelity quantum manipulation, it is necessary to suppress residual geometric dephasing. Fortunately, more and more work have begun to investigate the geometric contribution to dephasing [18–20]. And new schemes were recently proposed to suppress the residual geometric dephasing [21].

In this letter, we investigate the geometric dephasing under classical Ornstein-Uhlenbeck (OU) [22] fluctuating field using a quantum two-level system (TLS) in a trapped ion. Utilizing

* Corresponding authors.
E-mail addresses: hyf@ustc.edu.cn (Y.-F. Huang), zwzhou@ustc.edu.cn (Z.-W. Zhou), cfli@ustc.edu.cn (C.-F. Li).

https://doi.org/10.1016/j.scib.2019.09.007
2095-9273/

modified dynamical decoupling schemes such as Spin Echo (SE) and Carr-Purcell-Meiboom-Gill (CPMG) [21], we suppress the residual geometric dephasing effectively. Furthermore, by altering the intensity and correlation time of noise, we demonstrate the scope of application of these schemes in real experiments.

2. Experimental

2.1. Geometric phase of a qubit

Consider a TLS exposed to a slowly varying magnetic field, the Hamiltonian (setting $\hbar = 1$) for such a system is $H_1 = \mathbf{B}\cdot\boldsymbol{\sigma}/2$, where $\boldsymbol{\sigma} = (\sigma_x, \sigma_y, \sigma_z)$ are the Pauli operators, $\mathbf{B}$ is the magnetic field vector, expressed in units of angular frequency. This Hamiltonian can be simulated by a microwave driven hyperfine qubit of a trapped ion, where fast and accurate control of the magnetic field $\mathbf{B}$ is achieved through phase and amplitude manipulation of the microwave radiation coupled to the hyperfine qubit. The qubit Hamiltonian [8] in the frame rotating at the frequency of microwave drive ω_{mw} is

$$H_2 = \frac{1}{2}(\Delta\sigma_z + \Omega\sin\varphi\sigma_x + \Omega\cos\varphi\sigma_y), \tag{1}$$

where $\Delta = \omega_0 - \omega_{mw}$ is the detuning between the microwave drive frequency (ω_{mw}) and qubit transition frequency (ω_0), Ω is the Rabi frequency related to the intensity of the drive, and φ is the phase of drive. This Hamiltonian is equivalent to H_1 as we can regard $\mathbf{B} = (\Omega\sin\varphi, \Omega\cos\varphi, \Delta)$ as the magnetic field applied to TLS. Here $\mathbf{B}$ forms an angle $\theta = \arctan\frac{\Omega}{\Delta}$ with the z axis in the Bloch sphere. By changing the phase of microwave, the magnetic field precesses around this axis with palstance $\dot{\varphi}$ as shown in Fig. 1a. If the $\dot{\varphi}$ is small enough, usually satisfying the requirement that the adiabatic parameter $A = \dot{\varphi}\sin\theta/2B \ll 1$ for the case of constant angle θ [8], dynamical phase and geometric phase will be accumulated in the duration of this process. In order to observe pure Berry phase, one usually takes advantage of the SE technique to eliminate the part of dynamic phase as shown in Fig. 1b.

2.2. Dephasing in dynamic evolution of Hamiltonian

In order to introduce dephasing, we add additional noise in detuning in Eq. (1). Now let's consider the Hamiltonian under classical OU processes fluctuating field. OU process is a stationary Gauss-Markov process and a prototype of a noisy relaxation process. Many theoretical simulation and experimental investigation of Berry phase and holonomic quantum computation use Ornstein-Uhlenbeck stochastic process as a good analogy of realistic control noise [23–27]. An OU process noise $\mathbf{K}(t)$ with Lorentzian spectrum of bandwidth Γ and noise power α, displays the power spectrum $S(\omega) = 2\alpha\Gamma/(\Gamma^2 + \omega^2)$. Because decoherence in trapped ions platform is mainly from destabilization of environmental magnetic, i.e., noise in detuning Δ. We assume that the fluctuating noise $\mathbf{K}(t) = (0, 0, K_3)$, which is mainly the detuning noise and is independent of the controllable field $\mathbf{B}(t)$. This assumption results in the Hamiltonian

$$H_3 = \frac{1}{2}((\Delta + K_3)\sigma_z + \Omega\sin\varphi\sigma_x + \Omega\cos\varphi\sigma_y). \tag{2}$$

Due to the classical fluctuation field, the geometric phase exhibits a statistical distribution and this would cause dephasing. In the adiabatic limitation, the noise fluctuation and palstance are much smaller, that is $|K_3(t)| \ll |\mathbf{B}|$ and $|\dot{\varphi}| \ll |\mathbf{B}|$, we can define coherence function [28]

$$W = \langle e^{i\phi}\rangle = e^{-\langle\phi^2\rangle}, \tag{3}$$

in which [21]

$$\phi = -\sum_{k=1}^{n}\int_{T_{k-1}}^{T_k} s_k(\cos\theta - \dot{\varphi}\sin^2\theta/|\mathbf{B}|)K_3(t)dt. \tag{4}$$

(T_{k-1}, T_k) is the time segment cut apart by the π swapping pulses in dynamic decoupling sequences, s_k is eigenvalue of Hamiltonian H_2 in the kth time interval. The phase ϕ represents the dephasing in the whole dynamic process. The W will be less than one, which means dephasing due to existence of the noise once ϕ does not equal to zero. The term $s_k\cos\theta$ gives rise to the dynamic dephasing while the second term $-s_k\dot{\varphi}\sin^2\theta/B$ induces the geometric dephasing in Eq. (4) [21].

2.3. Suppressing residual geometric dephasing

If we can make the sum of integration in Eq. (4) become zero, both dynamic and geometric dephasing will be eliminated in principle. As demonstrated in Ref. [21], there are two schemes to solve this problem, as illustrated below:

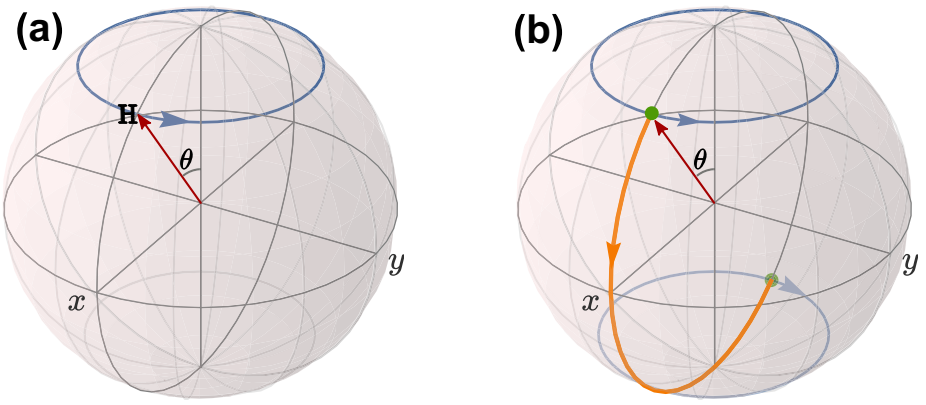

Fig. 1. (Color online) Dynamics of Hamiltonian **H** in Bloch sphere and corresponding geometric phase. The start point and end point of the trajectory of segment are represented by the green dots. The blue arrow and solid lines represent the direction and trajectory of Hamiltonian. The magenta arrows mark the angle between Hamiltonian and z axis in the evolution process. The swap of eigenstate of Hamiltonian after π pulse is represented by shallow orange arrow. (a) The Hamiltonian **H** tilted by an angle $\theta = \arctan\frac{\Omega}{\Delta}$ from z axis precesses about z axis with palstance $\dot{\varphi}$. Eigenstates of the Hamiltonian will accumulate dynamic phase γ_d and geometric phase γ_g in this process. (b) Spin echo strategy in which the Hamiltonian rotate in the opposite direction after a π swapping pulse, will result in elimination of dynamic phase and acquire pure geometric phase in eigenstates of the Hamiltonian. The phase of swapping π pulse is equal to the final phase of evolution of Hamiltonian plus $\pi/2$.

(1) In traditional dynamic decoupling schemes, such as Spin Echo and CPMG sequences, the neighbouring evolution part seperated by swapping π pulse have the same angle θ, so the ϕ would not be zero. But in this modified scheme, we vary the angle θ in neighboring adiabatic paths as shown in Fig.2a (SE sequences) and Fig. 2b (CPMG sequences). For the convenience of understand, we illustrate this scheme using modefied SE sequence. The Hamiltonian evolves 2π angle around z axis in Bloch sphere anticlockwise with angle θ_α, then a swapping π pulse whose phase is equal to the final phase of evolution of Eq. (1) plus $\pi/2$ is used to exchange the eigenstate of Hamiltonian. Finally, another evolution 2π angle clockwise with angle θ_β is implemented. By carefully designing these two angles, we can make the following equation hold:

$$\left(\cos\theta_\alpha - \frac{\dot{\varphi}_+ \sin^2\theta_\alpha}{B}\right) + \left(-\cos\theta_\beta + \frac{\dot{\varphi}_- \sin^2\theta_\beta}{B}\right) = 0, \qquad (5)$$

where $\dot{\varphi}_{+(-)}$ refers to the clockwise (anti-clockwise) angular velocity of Hamiltonian on the Bloch sphere (see Fig. 2a and b). Substitute Eq. (5) into (4) can receive the result $\phi \simeq 0$, which indicates there is no dephasing. It is noteworthy that since we use different slant angle for two adiabatic paths, the final Berry phase depends on these two angles, that is $\delta = 2\pi\cos\theta_\alpha + 2\pi\cos\theta_\beta$.

(2) To ensure that the Berry phase does not depend on two angles θ_α and θ_β, in the second scheme we separate two adiabatic paths of SE sequences into four parts separated by swapping π pulses, as shown in Fig. 2c. The Hamiltonian evolves π angle around z axis in Bloch sphere anticlockwise with angle θ, then a swapping π pulse exchanges the eigenstate of this Hamiltonian. Next the Hamiltonian will evolve a π angle clockwise with angle θ, which followed by another evolution clockwise with angle $\pi - \theta$. The second swapping π pulse will exchange the eigenstate of this Hamiltonian. Finally, a π angle evolution anticlockwise with angle $\pi - \theta$ will be implemented. In this scheme we can make the following equation hold:

$$\begin{aligned}&\left(\cos\theta - \frac{\dot{\varphi}_+ \sin^2\theta}{B}\right) + \left(-\cos\theta + \frac{\dot{\varphi}_- \sin^2\theta}{B}\right) + \\ &\left(-\cos\theta + \frac{\dot{\varphi}_+ \sin^2\theta}{B}\right) + \left(\cos\theta - \frac{\dot{\varphi}_- \sin^2\theta}{B}\right) = 0,\end{aligned} \qquad (6)$$

where $\dot{\varphi}_+ = -\dot{\varphi}_-$ refers to the clockwise (anti-clockwise) angular velocity of Hamiltonian on the Bloch sphere just as scheme one. These two schemes can ensure the integration ϕ in Eq. (4) to be zero, and both dynamic and geometric parts of dephasing will disappear.

We test these two schemes using a trapped $^{171}Yb^+$ ion in needle trap with the setup similar to the one described in Ref. [29]. The TLS is structured by two hyperfine levels of the $^{171}Yb^+$ ion in the $S_{1/2}$ ground-state, with $|0\rangle \equiv |^2S_{1/2}, F = 0, m_F = 0\rangle$ and $|1\rangle \equiv |^2S_{1/2}, F = 1, m_F = 0\rangle$, as shown in Fig. 3.

3. Results and discussion

In our experiment, Berry phase and coherence of the qubit have been measured as a function of angle spanned by the Hamiltonian and z axis. Using a SE pulses sequences, in which dynamic phase will be eliminated by opposite loop direction of neighboring adiabatic evolution, we can measure pure Berry phase. The modified

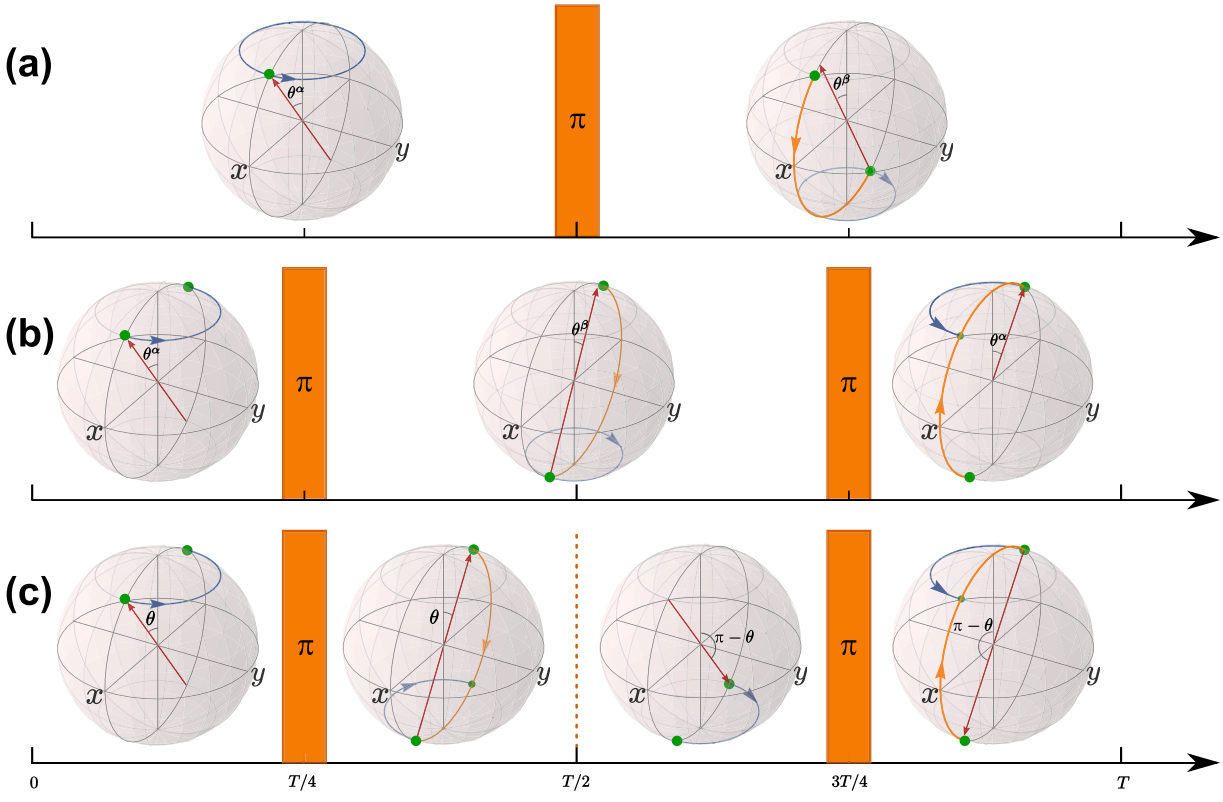

Fig. 2. (Color online) Trajectory of Hamiltonian of modified dynamic decoupling sequences in Bloch sphere. The start point and end point of the trajectory of segment are represented by the green dots. π swapping pulse is represented by the orange post. The blue arrow and solid lines represent the direction and trajectory of Hamiltonian. The magenta arrows mark the angle between Hamiltonian and z axis in the evolution process. The swapping of eigenstate of Hamiltonian after π pulse is represented by shallow orange arrow. Two examples of scheme one are shown in (a) modified SE strategy: the Hamiltonian evolves with angle θ_α with z axis in Bloch sphere anticlockwise initially and with angle θ_β clockwise after a π swapping pulse. (b) modified CPMG strategy: the Hamiltonian evolves half round with angle θ_α anticlockwise initially, and evolves a circle with angle θ_β clockwise after a swapping π pulse. Finally an evolution with angle θ_α anticlockwise half round is implemented. Scheme two is shown in (c).

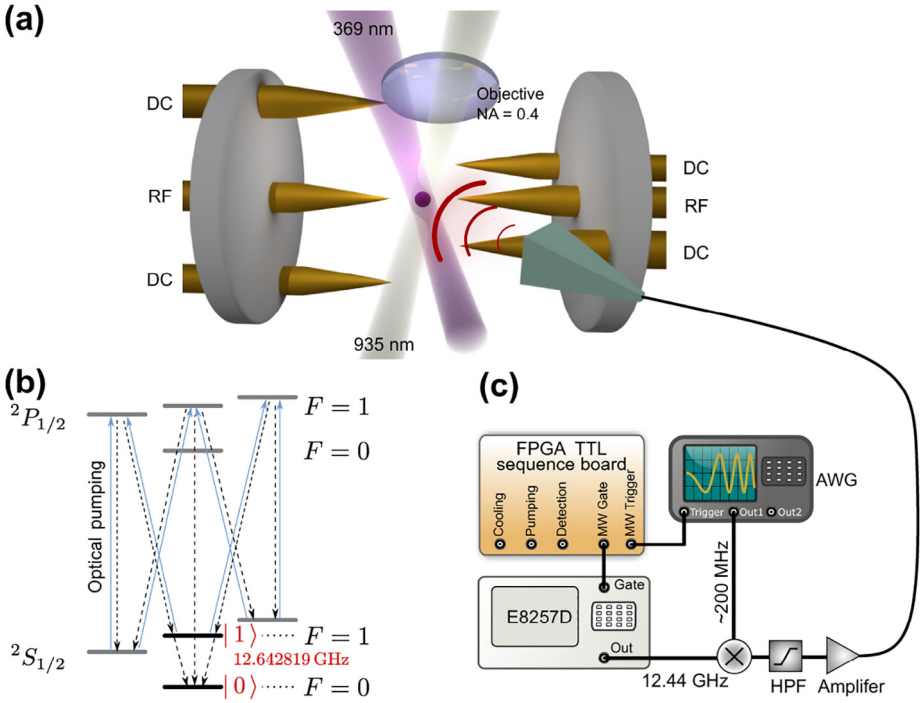

Fig. 3. (Color online) Experimental setup. (a) Needle trap used in experiment. A single $^{171}Yb^+$ ion is trapped in the trap. (b) Energy levels diagram of $^{171}Yb^+$ ion. Qubit state $|0\rangle$, $|1\rangle$ are mapped onto $|F = 1, m_F = 0\rangle, |F = 0, m_F = 0\rangle$ in the $S_{1/2}$ ground state manifold, respectively. The transition frequency between $|0\rangle$ and $|1\rangle$ is $(2\pi)12.642819$ GHz. (c) Mixing wave scheme to drive the trapped ion qubit. AWG: arbitrary wave generator, HPF: high pass filter.

Spin Echo experiment in scheme one takes the following process: After 1 ms Doppler cooling, the state of the ion is initialized to $|0\rangle$ by 20 μs optical pumping [30]. Then a series of coherent manipulations are implemented using microwave pulses ω_{mw} through a microwave horn. In order to observe different Berry phase with different angle θ, we vary ω_{mw} around qubit transition frequency $\omega_0 = 12.64$ GHz, which will cause different $\theta = \arctan\frac{\Omega}{\Delta}$. The 2π time for Rabi oscillation is adjusted to 95 μs, that is, the Rabi frequency $\Omega = 10.5$ kHz. The complete sequences start by preparing the superposition state of $|0\rangle$ and $|1\rangle$ with a $\pi/2$ resonant microwave. Then the Hamiltonian traces around z axis adiabaticly with angle θ_α by varying φ, the phase of microwave in Eq. (1) slowly, causing one of the eigenstate $|+\rangle$ of H_2 acquiring a phase $\gamma_+ = -\gamma_d + \gamma_{g+}$, $|-\rangle$ acquiring a phase $\gamma_- = \gamma_d + \gamma_{g-}$. γ_d and γ_g are dynamic and geometric phase respectively, $\gamma_{g+} = \pi(1 + \cos\theta)$ and $\gamma_{g-} = \pi(1 - \cos\theta)$. We make $\dot{\varphi}/B = 0.1$, which guarantees the adiabatic parameter $A = 0.05\sin\theta \ll 1$. A resonant π pulse then swaps the eigenstates of Hamiltonian in Eq. (1), after which the magnetic field traces along opposite direction with angle θ_β, causing the eigenstate $|+\rangle$ of H_2 acquiring $\gamma_+ = \gamma_d - \gamma_{g-}$, $|-\rangle$ acquiring $\gamma_- = -\gamma_d - \gamma_{g+}$. Finally the pure geometric phase difference between these two eigenstates is $\delta = 2\gamma_{g-} - 2\gamma_{g+} = -2\pi\cos\theta_\alpha - 2\pi\cos\theta_\beta$.

In experiment, K_3 noise is generated by means of adding synthetic stochastic components in the detuning term Δ in microwave drive. The noise applied to qubit conforms an OU process (detailed in the Appendix) with correlation time $\tau = 10$ s and intensity $\alpha/\Omega^2 \approx 1$. In order to simulate the statistical stochastic effect of noise, the same experiment is done with different OU noise sequence generated using different random seed. Every experiment was done 100 times to obtain the average probability value. We get density matrix ρ of final state by state tomography (detailed in the Appendix) and calculate the coherent function and Berry phase according to $\delta = \arg\langle\rho_{0,1}(T)\rangle$ and $W = |\langle\rho_{0,1}(T)\rangle|/|\rho_{0,1}(0)|$, where $\langle\cdots\rangle$ represent the average of all noise implementation. In Fig. 4a, we measure the dephasing of SE and CPMG sequences in the case of low-frequency noise $\Gamma T \ll 1$, in which $\Gamma = 1/\tau$ and T is the total time of adiabatic evolution. The parameter θ is changed from 0 to $\pi/2$ because the angle $\theta = 0$ is the same as $\theta = \pi$ in these modified schemes and what we focus is the ratio of the noise in detuning rather than the sign of the detuning. Obviously, SE and CPMG methods only suppress the dephasing effectively in small angle θ. When it comes to bigger angle, such as $\theta > \pi/4$, these two methods fail. It can be understood easily because the ratio K_3/Δ is bigger in larger angle θ and the K_3 noise will cause bigger impact. The dephasing of these two dynamic decoupling schemes in large angle is mainly due to geometric dephasing. This can be seen from the second term in Eq. (4), which indicates geometric dephasing increases with incremental angle θ. In order to suppress the residual geometric dephasing, we modify the SE and CPMG sequences according to the above-mentioned methods exhibited in Fig. 2. The results are shown in Fig. 4b, in which modefied dynamic decoupling sequences (SE-scheme1, CPMG-scheme1 and scheme2) suppress residual dephasing successfully even in large angle θ. If we define dephasing rate $\chi = -\frac{\log_{10}W}{T}$, the dephasing rate will be reduced up to one order of magnitude in large θ after using modified schemes compared with traditional dynamic decoupling sequences as shown in Fig. 4c. Meanwhile, Berry phases acquired by all these schemes are in accordance with theoretical predictions as shown in Fig. 4d and e. The theoretical predictions are calculated by numerical simulation of Eq. (2) with the Monte Carlo method.

In the motivation of realistic applications in QIP, we further investigate the performance of these modified methods, under different parameters τ and α of Gaussian noise at $\theta = 9\pi/20$. First, we vary the bandwidth Γ from 10^{-1} to 10^4 Hz with fixed parameter $\alpha/\Omega^2 \approx 1$. The results are shown in Fig. 4f, which indicate that these methods become invalid along with increasing correlation time $1/\Gamma$ of the noise. Especially, when $\Gamma > 100$ Hz, dephasing

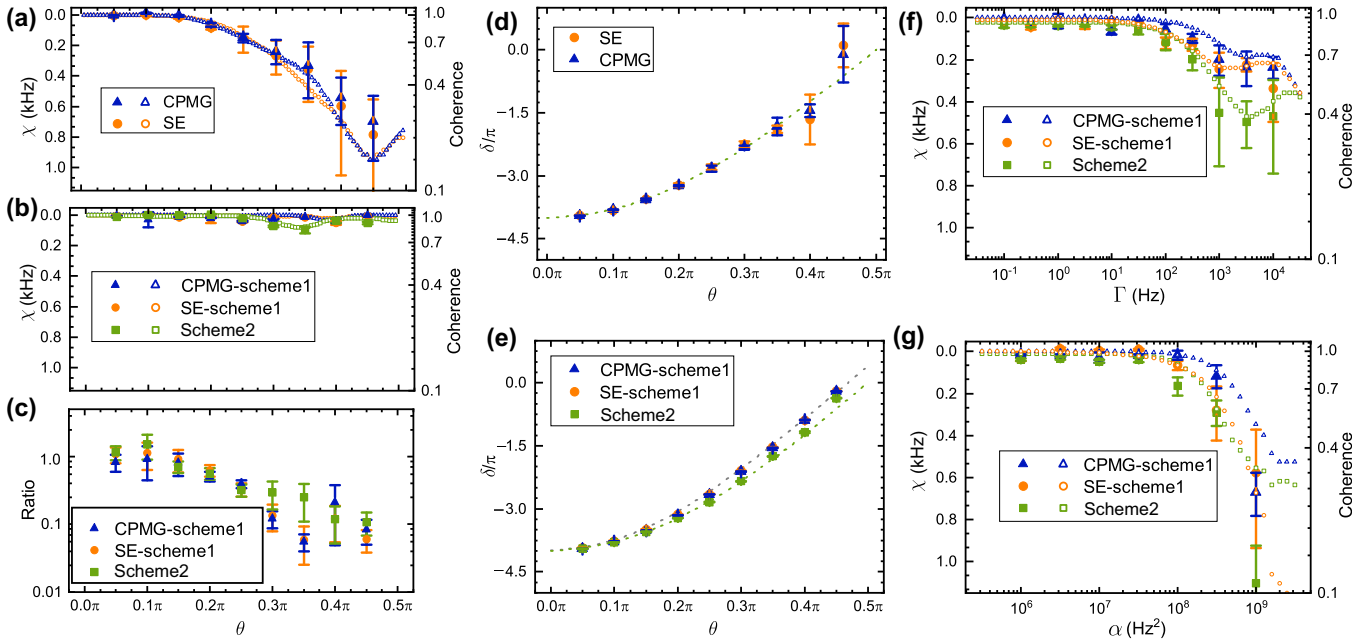

Fig. 4. (Color online) Performance comparison between the classical and modified dynamic decoupling protocols under Gaussian noise on experiment. Two classical protocols (SE (orange circle) and CPMG (blue triangle)) and three modified protocols (SE-scheme1 (orange circle), CPMG-scheme1 (blue triangle) and scheme 2 (green square)) are studied. The hollow markers indicate the numerical simulation data and the solid markers indicate experimental data. (a), (b) Measured dephasing rate and coherence as a function of angle θ with the classical and modified dynamic decoupling protocols, respectively. All of the classical schemes become invalid in large angle θ, while all the modified schemes can suppress dephasing even in large angle θ. (c) Dephasing rate ratio between the modified schemes and classical decoupling protocols. (d), (e) Berry phase measured in classical and modified dynamic decoupling protocols, respectively. The dashed lines are the theoretical Berry phase difference $-4\pi\cos\theta$ (green) and modified protocol scheme1 Berry phase difference $-2\pi\cos\theta_\alpha - 2\pi\cos\theta_\beta$ (gray). (f) Coherence of the qubit measured in modified decoupling protocols with fixed intensity of noise $\alpha \cong \Omega^2$. The modified schemes work effectively when Γ<100 Hz. (g) Coherence of the qubit of modified decoupling protocols with fixed correlation time τ = 0.01 s. The error bars indicate the standard deviation by statistic treatment of the measured data with 100 realizations of noise.

begins to be notable and these schemes begin to be ineffective. Second, we fix $\tau = 0.01$ s and change α to make the ratio α/Ω^2 to vary from 0.01 to 10. The coherence of the qubit is shown in Fig. 4g. The bigger the ratio α/Ω is, the worse the effect of these methods will be. Fortunately, the correlation time of magnetic field noise is usually larger than 0.01 s and the intensity of noise usually less than Ω^2 [31,32]. So these two schemes will still be very useful in many scenes.

4. Conclusion

In our work, we studied the dephasing of a TLS under Gaussian noise using a single trapped ion. Under this situation, OU type of noise is considered to the classical fluctuating field, which roughly corresponds to the treatment for the second-order time-convolution in the framework of quantum open system [33]. However, our treatments cannot be applied directly to the main equation. Because, the feature of the pure state of the system cannot be preserved in the framework of the main equation. How to generalize the geometric phase operations for a generic open quantum system based on microscopic models remains extraordinary attractive. Some novel progresses on geometric phase in non-Markovian open systems have been made [34,35].

In summary, we experimentally investigate suppressing the residual geometric dephasing effectively by utilizing modified dynamic decoupling sequences. In contrast with traditional dynamic decoupling schemes, these modified schemes can reduce dephasing rate more than one order of magnitude. The measurement results share well agreement with theoretical simulations. In addition, we also discuss effects of these sequences in different intensities and correlation times of noise, and make sure that it will reduce the interference between quantum systems and environment in most laboratory environment. It will be helpful for precise quantum state manipulation in realistic experiments of QIP.

Conflict of interest

The authors declare that they have no conflict of interest.

Acknowledgments

This work was supported by the National Key Research and Development Program of China (2016YFA0302700), Anhui Initiative in Quantum Information Technologies (AHY070000), Key Research Program of Frontier Sciences, CAS (QYZDY-SSW-SLH003), National Natural Science Foundation of China (11474268, 11574294, 11734015, 11474270 and 11404319), the Fundamental Research Funds for the Central Universities (WK2470000026, WK2470000027 and WK2470000028), and the Anhui Provincial Natural Science Foundation (1608085QA22).

Author contributions

Zheng-Wei Zhou, Xiao-Ke Qin and Tao Tu devised this proposal. Jin-Ming Cui, Ming-Zhong Ai and Yun-Feng Huang designed the experiments. Jin-Ming Cui and Ming-Zhong Ai performed the experiments. Ran He and Zhong-Hua Qian analyzed the data. Jin-Ming Cui, Ming-Zhong Ai, Chuan-Feng Li and Guang-Can Guo wrote the manuscript. All the authors contributed to the general discussion.

Appendix A. Classical OU fluctuating noise in experiment

The OU process has a long history and has many applications in physics. For example, it has been used to describe Brownian motion and Johnson noise [36]. Many investigators used the OU process as a model of "colored noise" [37]. In many Markov processes about a "stable state", the fluctuations can approximately be described as an OU process if those fluctuations are sufficiently small enough. It can be understood to be the universal Markov process K that evolves with time t according to the following equation [22]:

$$\frac{\mathrm{d}K(t)}{\mathrm{d}t} = -\frac{1}{\tau}K(t) + c^{1/2}G(t), \tag{A1}$$

in which τ and c are positive constants called respectively, the correlation time and the diffusion constant, and $G(t)$ is Gaussian white noise. An exact updating formula for K by itself is [38]

$$K(t+\Delta t) = K(t)\mathrm{e}^{-(1/\tau)\Delta t} + \left[\frac{c\tau}{2}(1-\mathrm{e}^{-(2/\tau)\Delta t})\right]^{1/2} n, \tag{A2}$$

and n represents a sample value of the unit normal random variable $N(t) = \mathcal{N}(0,1)$.

We generate the Gaussian noise according to Eq. (A2) in experiments. In order to acquire statistical average results, 100 times experiments are implemented using different statistical random seed in every experiment data point. The $K(t)$ noise signal is added to constant carrier frequency ω_0 using arbitrary waveform generator (AWG).

Appendix B. Tomography and SPAM error

The state of the qubit is determined in a deatructive readout through the resonant fluorescence and reconstructed using state tomography. Any single-qubit density matrix $\hat{\rho}$ can be uniquely represented by four parameters $\{S_0, S_1, S_2, S_3\}$ [39]:

$$\hat{\rho} = \frac{1}{2}\sum_{i=0}^{3} S_i \hat{\sigma}_i, \tag{B1}$$

the $\hat{\sigma}_i$ matrices are

$$\hat{\sigma}_0 = \begin{pmatrix} 1 & 0 \\ 0 & 1 \end{pmatrix},\ \hat{\sigma}_1 = \begin{pmatrix} 0 & 1 \\ 1 & 0 \end{pmatrix},\ \hat{\sigma}_2 = \begin{pmatrix} 0 & -i \\ i & 0 \end{pmatrix},\ \hat{\sigma}_3 = \begin{pmatrix} 1 & 0 \\ 0 & -1 \end{pmatrix}, \tag{B2}$$

and the S_i values are given by $S_i = \mathrm{Tr}\{\hat{\sigma}_i\hat{\rho}\}$. We measure these four parameters according to a specific pair of projective measurements:

$$\begin{aligned} S_0 &= P_{|0\rangle} + P_{|1\rangle}, \\ S_1 &= P_{\frac{1}{\sqrt{2}}(|0\rangle+|1\rangle)} - P_{\frac{1}{\sqrt{2}}(|0\rangle-|1\rangle)}, \\ S_2 &= P_{\frac{1}{\sqrt{2}}(|0\rangle+i|1\rangle)} - P_{\frac{1}{\sqrt{2}}(|0\rangle-i|1\rangle)}, \\ S_3 &= P_{|0\rangle} - P_{|1\rangle}, \end{aligned} \tag{B3}$$

where $P_{|\psi\rangle}$ is the probability to measure the state $|\psi\rangle$. Then the density matrix of final state can be reconstructed according to Eq. (B1).

Besides, we measured the state preparation and measurement (SPAM) error of the qubit. The dark error, mainly due to dark count of the photo-multiplier (PMT), is about 0.003. And the bright error is 0.009, which is mainly from the collection efficiency of objective.

References

[1] Berry MV. Quantal phase factors accompanying adiabatic changes. Proc R Soc Lond A 1984;392:45–57.
[2] Arai K, Lee J, Belthangady C, et al. Geometric phase magnetometry using a solid-state spin. arXiv:180307176, 2018.
[3] Cai H, Ren Z. Geometric phase for a static two-level atom in cosmic string spacetime. Classical Quant Grav 2018;35:105014.
[4] Aharonov Y, Anandan J. Phase change during a cyclic quantum evolution. Phys Rev Lett 1987;58:1593.
[5] Tong DM, Sjöqvist E, Kwek LC, et al. Kinematic approach to the mixed state geometric phase in nonunitary evolution. Phys Rev Lett 2004;93:080405.
[6] Carollo A, Fuentes-Guridi I, Santos MF, et al. Geometric phase in open systems. Phys Rev Lett 2003;90:160402.
[7] Jones JA, Vedral V, Ekert A, et al. Geometric quantum computation using nuclear magnetic resonance. Nature 2000;403:869.
[8] Leek PJ, Fink JM, Blais A, et al. Observation of berry's phase in a solid-state qubit. Science 2007;318:1889–92.
[9] Möttönen M, Vartiainen JJ, Pekola JP. Experimental determination of the berry phase in a superconducting charge pump. Phys Rev Lett 2008;100:177201.
[10] Zhang Y, Tan YW, Stormer HL, et al. Experimental observation of the quantum hall effect and berry's phase in graphene. Nature 2005;438:201.
[11] Chen XY, Li T, Yin ZQ. Nonadiabatic dynamics and geometric phase of an ultrafast rotating electron spin. Sci Bull 2019;64:380–4.
[12] Filipp S, Klepp J, Hasegawa Y, et al. Experimental demonstration of the stability of berry's phase for a spin-1/2 particle. Phys Rev Lett 2009;102:030404.
[13] Richardson DJ, Kilvington AI, Green K, et al. Demonstration of berry's phase using stored ultracold neutrons. Phys Rev Lett 1988;61:2030.
[14] Leibfried D, DeMarco B, Meyer V, et al. Experimental demonstration of a robust, high-fidelity geometric two ion-qubit phase gate. Nature 2003;422:412.
[15] Harty TP, Allcock DTC, Ballance CJ, et al. High-fidelity preparation, gates, memory, and readout of a trapped-ion quantum bit. Phys Rev Lett 2014;113:220501.
[16] Ballance CJ, Harty TP, Linke NM, et al. High-fidelity quantum logic gates using trapped-ion hyperfine qubits. Phys Rev Lett 2016;117:060504.
[17] Schlosshauer MA. Decoherence: and the quantum-to-classical transition. Springer Science & Business Media; 2007.
[18] Whitney RS, Makhlin Y, Shnirman A, et al. Geometric nature of the environment-induced berry phase and geometric dephasing. Phys Rev Lett 2005;94:070407.
[19] Berger S, Pechal M, Kurpiers P, et al. Measurement of geometric dephasing using a superconducting qubit. Nat Commun 2015;6:8757.
[20] Berger S, Pechal M, Abdumalikov Jr AA, et al. Exploring the effect of noise on the berry phase. Phys Rev A 2013;87:060303.
[21] Qin XK, Guo GC, Zhou ZW. Suppressing the geometric dephasing of berry phase by using modified dynamical decoupling sequences. New J Phys 2017;19:013025.
[22] Gillespie DT. Exact numerical simulation of the ornstein-uhlenbeck process and its integral. Phys Rev E 1996;54:2084.
[23] Brion E, Pedersen LH, Mølmer K, et al. Universal quantum computation in a neutral-atom decoherence-free subspace. Phys Rev A 2007;75:032328.
[24] Cai J, Naydenov B, Pfeiffer R, et al. Robust dynamical decoupling with concatenated continuous driving. New J Phys 2012;14:113023.
[25] Li JQ, Liang JQ. Quantum and classical correlations in a classical dephasing environment. Phys Lett A 2011;375:1496–503.
[26] De Chiara G, Palma GM. Berry phase for a spin 1/2 particle in a classical fluctuating field. Phys Rev Lett 2003;91:090404.
[27] Lupo C, Aniello P. Robustness of the geometric phase under parametric noise. Phys Scr 2009;79:065012.
[28] Bergli J, Galperin YM, Altshuler BL. Decoherence in qubits due to low-frequency noise. New J Phys 2009;11:025002.
[29] Cui JM, Huang YF, Wang Z, et al. Experimental trapped-ion quantum simulation of the kibble-zurek dynamics in momentum space. Sci Rep 2016;6:33381.
[30] Olmschenk S, Younge KC, Moehring DL, et al. Manipulation and detection of a trapped Yb^+ hyperfine qubit. Phys Rev A 2007;76:052314.
[31] Fluhmann C. Stabilizing lasers and magnetic fields for quantum information experiments. ETH Zurich, Master's thesis 2014.
[32] Ruster T, Schmiegelow CT, Kaufmann H, et al. A long-lived zeeman trapped-ion qubit. Appl Phys B 2016;122:254.
[33] Chen HB, Lambert N, Cheng YC, et al. Using non-markovian measures to evaluate quantum master equations for photosynthesis. Sci Rep 2015;5:12753.
[34] Luo DW, You J, Lin HQ, et al. Memory-induced geometric phase in non-markovian open systems. Phys Rev A 2018;98:052117.
[35] Luo DW, Lin HQ, You J, et al. Geometric decoherence in diffusive open quantum systems. arXiv:190606404, 2019.
[36] Gillespie D. The mathematics of brownian motion and johnson noise. Am J Phys 1996;64:225.
[37] Castro F, Sanchez A, Wio H. On reentrance phenomena in noise induced transitions. Phys Rev Lett 1995;75:1691.
[38] Gillespie DT. Markov processes: an introduction for physical scientists. Elsevier; 1991.
[39] Altepeter JB, James DF, Kwiat PG. 4 qubit quantum state tomography. In: Quantum state estimation. Springer; 2004. p. 113–45.

Jin-Ming Cui got his B.S. degree from University of Science and Technology of China (USTC) in 2008, and received his Ph.D. degree from USTC in 2013. During his Ph.D.'s study, he focused on experiment works with optical micro-cavities and NV centers. Now he works as an associate researcher in USTC and his major research focuses on quantum information based on trapped ion system, including quantum simulation, quantum computation, quantum network and fiber Fabry-Perot microcavity.

Yunfeng Huang who got his Ph.D. degree in University of Science and Technology of China (USTC) in 2003, now is a professor in College of Physics, USTC. His main research interests in recent years involve trapped ion quantum computing and multi-photon quantum information processing experiments. For ion trap system, he is now focusing on building distributed ion trap quantum computer through high-efficiency photonic connection between distant ion traps.

Zhengwei Zhou received both his Bachelor degree (in 1996) and Ph.D degree (in 2001) in physics from the University of Science and Technology of China (USTC). He joined the faculty of CAS Key Laboratory of Quantum Information, USTC in 2001 and became a full professor in 2007. His research interests focus on quantum simulation, physical realization of quantum information processing, physics of cold atoms, and manipulation in the synthetic dimension systems.

Chuan-Feng Li is a Professor in University of Science and Technology of China. He received his Ph.D. degree (1999) from University of Science and Technology of China. His research field is quantum optics and quantum information. He is now focusing on constructing quantum network and exploring quantum physics with quantum technology.